Quieting a rib-framed honeycomb core sandwich panel for a rotorcraft roof

Stephen A. Hambric
ARL/Penn State University
PO Box 30
State College, PA 16804

Micah R. Shepherd
ARL/Penn State University
PO Box 30
State College, PA 16804

Noah H. Schiller
NASA Langley Research Center
Hampton, VA 23681

Royce Snider
Bell Helicopter-Textron
Fort Worth, TX 76101

Carl May
Bell Helicopter-Textron
Fort Worth, TX 76101

Abstract

A rotorcraft roof composite sandwich panel has been redesigned to optimize sound power transmission loss (TL) and minimize structure-borne sound for frequencies between 1 and 4 kHz where gear meshing noise from the transmission has the most impact on speech intelligibility. The roof section, framed by a grid of ribs, was originally constructed of a single honeycomb core/composite facesheet sandwich panel. The original panel has acoustic coincidence frequencies near 600 Hz, leading to poor TL across the frequency range of 1 to 4 kHz. To quiet the panel, the cross section was split into two thinner sandwich subpanels separated by an air gap. The air gap was sized to target the fundamental mass-spring-mass resonance of the panel system to less than 500 Hz, well below the frequency range of interest. The panels were designed to withstand structural loading from normal rotorcraft operation, as well as 'man-on-the-roof' static loads experienced during maintenance operations. Thin layers of viscoelastomer were included in the facesheet ply layups, increasing panel damping loss factors from about 0.01 to 0.05. Transmission loss measurements show the optimized panel provides 6-11 dB of acoustic transmission loss improvement, and 6-15 dB of structure-borne sound reduction at critical rotorcraft transmission tonal frequencies. Analytic panel TL theory simulates the measured performance within 3 dB over most frequencies. Detailed finite element (FE)/boundary element (BE) modeling simulates TL slightly more accurately, within 2 dB for frequencies up to 4 kHz, and also simulates structure-borne sound well, generally within 3 dB.

Introduction

Commercial rotorcraft are powered by drive systems comprised of complex transmissions. As the transmission gears rotate at high rates of speed, they induce vibrations and noise at Gear Meshing Frequencies (GMFs) in the transmission cavity above the cabin (see the example in Figure 1, and [1, 2] for a general discussion of transmission noise). Structural roof panels are driven acoustically and structurally by the GMF tones, radiating sound into the cabin. Composite materials are sometimes used to construct lightweight stiff panels for rotorcraft which meet structural integrity requirements, but also lead to increased interior sound radiation due to their reduced structural impedances and increased sound radiation efficiencies. Expensive and heavy acoustic treatments are therefore often added to the panels to reduce sound transmission. A more efficient and cost-effective noise control approach, however, is to better design the structural panel itself to minimize noise.

To characterize the structural-acoustic behavior of a typical sandwich roof panel, a notional design was constructed, as shown in Figure 2. A honeycomb core composite face sheet sandwich panel (see Figure 3) is mounted between a rectangular frame of large, stiff aluminum ribs which represent the roof rails (which run forward and backward) and the intercostal beams (which run side to side). The rotorcraft transmission mounts to the four corners of the rib frame. As shown in Figure 4, the center panel edges taper downward to pure face sheet stacks at the rib mounting points, which extend beyond the ribs. The structural-acoustic behavior of this ‘baseline’ panel has been evaluated computationally and experimentally previously [3]. The transmission loss (TL) of the baseline panel, measured in NASA Langley’s Structural Acoustics Loads

and Transmission (SALT) facility [4] and shown in Figure 5, is low (less than 25 dB) between 1-4 kHz, the frequency range most critical for speech communication, and where strong rotorcraft transmission tones typically occur. In particular, our application is most concerned with Bull and Pinion Gear Meshing Frequencies (GMFs) at 1 and 3 kHz emanating from a typical Bell Helicopter rotorcraft transmission. The sound transmission through the center panel, which has a low coincidence frequency of about 600 Hz, dominates the transmitted sound.

In this paper, we summarize the design of an optimized roof panel which increases TL through the center sandwich panel region between 1 and 4 kHz, and specifically near 1 and 3 kHz (the transmission GMF tones), but also does not violate several important design constraints, including:

- the areal density (mass/area) cannot exceed 5.7 kg/m^2,
- the thickness toward the cabin interior cannot exceed – 1.59 cm, and
- the structural materials must withstand limiting in-flight loads as well as 'man-on-the-roof' loading for maintenance operations.

These constraints preclude the use of methods suggested in the literature to soften the sandwich panel to shift coincidence frequency upward so that the well-known TL coincidence dip is higher than the frequency range of interest [5, 6]. Also, adding mass is clearly not an option due to the stringent weight requirement. Mass constraints are, of course, common in the aerospace community.

Three well known noise control procedures were applied to develop an optimized panel design without violating the design constraints:

- the center panel was split into two subpanels separated by an air gap,
- a blanket, also used for insulation and fire protection, was included in the air gap, and

- very thin viscoelastic layers (VHB 9469 adhesive from 3M) were embedded within the outer and inner face sheet assemblies to increase structural damping.

This paper summarizes the development of the optimized panel, including a brief assessment of the structural integrity calculations. Measurements of structure-borne and airborne sound transmission loss are shown, along with comparisons to analytic and computational estimates.

Panel Designs

The baseline panel is shown in Figure 2, and the optimized panel is shown in Figure 6. Schematics of the cross-sections of the baseline and optimized center panels are shown in Figure 7. A useful reference on the properties of honeycomb sandwich panels may be found in [7]. The final optimized panel balances acoustic performance with structural integrity constraints, as well as meeting weight and space goals. The split panel concept is augmented with damped face sheets which include embedded VHB viscoelastic material, and the gap is filled with a MicroLite blanket. The final surface density of the optimized center panel region is 5.5 kg/m^2, which is less than the upper limit of 5.7 kg/m^2. The baseline center panel surface density is 3.1 kg/m^2 without any added treatment packages. Typical treatment packages increase the surface density by 1-2.6 kg/m^2. Although the optimized panel is thicker than the baseline panel, the excess thickness is shifted to outside the fuselage, as shown in Figure 7. The extra thickness will not affect the transmission or other electrical, mechanical, or hydraulic elements in the roof cavity region of a typical rotorcraft.

The face sheets are made of layers of Cytec G30-500/5276-1 Carbon/Epoxy plain weave fabric, 0.2 mm (0.0079 in) thick, and the honeycomb cores are Hexcel

Kevlar (1/8" cell size, 3.3 lb/ft^3). The cores are sandwiched by inner and outer face sheets. The baseline panel uses 3-layer fabric plies with [0/45/0] orientations, where the '0' indicates fiber tows in the 0 and 90 degree directions (aligned with the edges of the overall panel) and the '45' indicates fiber tows in the + and – 45 degree directions. In this plain weave fabric, there are equal amounts of fiber tows in the warp and weft directions.

The edges of the baseline panel, which do not include honeycomb core, are stacks of 10 carbon/epoxy plies with orientation $[0/45/45/0/0]_S$, where 'S' indicates symmetry about the center ply for the remaining angles. The optimized panel edging has two additional outer plies, along with a layer of VHB material at the center (between plies 6 and 7), which weakens the effective flexural elastic modulus of the cross section by about 20%. Selected properties of the panel materials are shown in Table 1. Note that the honeycomb core shear modulus is stiffer in the ribbon direction.

The frame is made from aluminum I-beams. The roof beams (horizontal in Figures 2, 4, and 6) are 1016 mm (40 inches) long, and the intercostal beams (vertical) are 762 mm (30 inches) long. The flange widths of the roof and intercostal beams are 76.2 mm (3 inches) and 50.8 mm (2 inches) respectively. All beams are 102 mm (4 inches) high, with 3.96 mm (0.156 inch) flange and web thicknesses. The roof beams and transverse intercostal beam webs are connected by aluminum shear clips, and the top flanges are connected by four aluminum splice straps at the joints which represent the transmission mounting points. The roof beams are connected to the panel with 5/16" diameter titanium protruding shear head pins and titanium collars spaced at a nominal 6.5D pitch. Additional structural details, including the tapered sections near the frame, are available in

[3].

Embedded Viscoelastomer

Thin layers of viscoelastomer are sandwiched between the layers of the facesheet sections of the optimized panel to increase structural damping, and therefore random incidence TL at and above the panel critical frequency. The face sheets used in these panels, however, are extremely thin and lightweight. In the prototypic baseline panel, each sheet is comprised of only three layers of 0.2 mm thick carbon fabric (0/45/0 degree orientations). Replacing the center layer with viscoelastomer requires similarly thin and light damping material. We used 3M's VHB 9469 adhesive, which is 0.13 mm thick, of comparable mass density, and is formulated to have high damping properties near room temperature and at frequencies between 1 and 4 kHz. However, replacing the center layer of each face sheet with a layer of the VHB material leaves only outer and inner carbon layers with 0 and 90 degree ply orientations, reducing face sheet net stiffness.

Young's Moduli (computed assuming a Poisson's ratio of 0.499) and loss factors for VHB 9469 are compared at 20 and 30 degrees C in Figure 8. The loss factors are quite high, ranging between 0.7 and 1.1 between 1 and 4 kHz. The net damping benefits of the VHB material were checked by performing experimental modal analyses on two test coupon panels. The coupon panel dimensions (48 cm x 58 cm) were chosen to avoid modal degeneracy, so that each structural mode is distinct in frequency and easily identified. Hexcel Kevlar core (1.27 cm thick) was used for the test coupon cores. The two coupon panels were constructed using different approaches. In the first panel, the carbon fabric and VHB were cocured, such that part of the VHB fused with the epoxy in the carbon fabric sheets. This formed a hybrid structure with uncertain properties. A second panel with

pre-cured carbon fabric sheets post-bonded with the VHB was also constructed.

Complex modes were extracted from experimental modal analysis data, and loss factors and resonance frequencies were compared for the two panels. Figure 9 compares the modal loss factors for the two panels for frequencies up to about 5 kHz. The post-bond approach consistently yields higher damping, and both construction approaches lead to strong damping improvements at 1 and 3 kHz, where the dominant transmission tones occur. The cocuring process likely reduced the amount of VHB between the face sheets (with some of the VHB being absorbed into the sheets), thereby reducing the strain energy dissipated in the VHB layer. Based on these data, the post-bond approach was used for the optimized panel.

Replacing the center carbon layer reduces the face sheet stiffness, thereby reducing the flexural wavespeeds. The measured mode shapes were used to estimate modal wavenumbers, which were combined with modal frequencies to determine the modal wavespeeds. The modal wavespeeds were then used to infer an effective face sheet in-plane Young's Modulus 30% of that of the baseline panel. Details of this procedure are provided in [3, 8]. The reduced stiffness and wavespeeds lead to higher acoustic coincidence frequencies, which must be monitored to ensure they do not align with the targeted reduction frequencies of 1 and 3 kHz. Here, the targeted coincidence frequency of the optimized panel section is about 2 kHz.

The test coupons also provided an opportunity to verify the FE modeling procedure for sandwich panels with layers of VHB material. Figure 10 shows a schematic of the cross-sectional modeling of the panels. The coupons were modeled with 4,370 quadratic solid elements. Each ply layer was modeled with

one element through its thickness, and four elements represent the Kevlar core. The ribbon direction was modeled along the length of the panel. The adhesive layers between the inner plies and the core were not modeled explicitly, but the layer masses were simulated instead by increasing the adjacent ply surface mass densities. The final modeled and measured weights match almost exactly.

The viscoelastomer Young's Moduli were varied over several center frequencies per the data shown in Figure 8. Complex modes were extracted using the commercial FE software NASTRAN for each property set, and modal frequencies were determined based on proximity to the center frequency of each set. Figure 11 compares the measured and simulated resonance frequencies, which agree to within +-4%. Figure 12 compares measured and simulated structural loss factors, which agree well for frequencies above 1 kHz. Below 1 kHz, the simulated loss factors are higher than the measured ones. However, since this project focuses on frequencies between 1 and 4 kHz, we have not pursued the cause of this discrepancy. Overall, the good agreement between measured and predicted resonance frequencies and loss factors confirm the modeling procedure and the underlying material properties.

Air gap sizing and fill

The 12.7 mm (0.5 inch) gap between subpanels was chosen to ensure that sound transmission degradation associated with the well-known mass-spring-mass resonance of a double panel system is well below 1 kHz. This resonance frequency, where each panel acts as a lumped mass connected by the stiffness of the air gap, is:

$$f_o = \frac{1}{2\pi}\sqrt{\frac{\rho c^2 / d}{m_1 m_2 / (m_1 + m_2)}}, \qquad (1)$$

where ρc^2 is the bulk Modulus of air, d is the air gap thickness, ρ is the air mass density, c is the speed of sound, and m_1 and m_2 are the two outer panel area densities. In the equation, the numerator represents the air gap stiffness per unit area, and the denominator represents the effective total panel mass per unit area. This resonance amplifies the sound transmission through the double panel system at and around its resonance frequency. The effects of the gap thickness on the mass-spring-mass resonance, and on the overall panel thickness, are summarized in Table 2. A 12.7 mm gap shifts the resonance below 500 Hz, which is sufficiently low so that TL degradation should not occur above 1 kHz.

Rather than leave the air gap empty, it is filled with a 9.5 mm (0.375 inch) thick layer of Amber Microlite AA insulation (24 kg/m^3). The Microlite blanket provides thermal insulation, as well as reduced sound transmission through its added mass. It is common to add an extra layer of Microlite contained within a thin plastic covering on the inside surfaces of current rotorcraft roof panels. However, the layers are costly, and must often be removed when servicing the panels. Including the insulation inside the panel is preferable. The added acoustic transmission loss benefits are modest, and are due to the added mass of the material, as shown in Table 3. Standard ‘mass law’ TL calculations [3] were used to compare to the values provided by the vendor.

Structural integrity FE modeling and analysis

The optimized panel was modeled using finite elements, as shown in Figure 13. Each ply of fabric and each layer of VHB was discretely modeled with a single layer of elements through the thickness. Each core was modeled with two elements through the thickness. Adhesive plies were not included in the model, as they have negligible effect on the structural performance of the panel. Beams,

straps and angle brackets were used to represent the support structure of a prototypic roof frame. The brackets, straps, beams, and panel are connected with fasteners. These elements are connected together in the FE model using spring elements at the fastener locations. The nominal smeared material properties are listed in Table 1.

While we are focused mostly on the acoustic performance of the panel, it is still necessary to analyze the panel structural integrity using critical design loads for representative rotorcraft roof panels. Skin panel strength (including debonding of face sheets from the core), ramp strength (the transition region between the center panel and the frame), edgeband fiber and bearing strength, panel stability and step load (man-on-the-roof) response were analyzed. Upper skin applied ultimate loads were based on 150% of limit flight loads and were used to analyze the critical skin region using an elevated temperature wet open hole compression allowable. The edgeband fiber strength analysis is similar to the skin panel strength analysis, except that the loading moment is applied directly to the edgeband. The edgeband bearing strength was assessed for ‘jump takeoff’ load conditions. To assess buckling, the panel was held fixed at the frame and critical loads and moments were applied. The resulting critical buckling eigenvalues are both greater than 1.0, demonstrating that the plies in the ramp will provide adequate stability under worst case operating conditions. Finally, a 272 kg (600 lb) man-on-the-roof load was applied to the center of the panel. A nonlinear static analysis was run which shows that the top panel will contact the bottom panel in this case, sharing the load between the panels. Assuming a worst-case deflection (shown in Figure 14), maximum stresses were computed and found to be within allowable limits. The maximum edge forces were then used to compute critical strains in the upper face

sheet, which were also found to be well within allowable limits. More details on structural integrity evaluations are in [3].

Transmission Loss Simulations and Measurements

For the baseline panel, TL was simulated using both traditional analytic infinite panel methods, and using a finite element (FE) model of the actual panel and a boundary element (BE) model of the air surrounding the panel. FE/BE approaches for simulating TL have been used successfully by other researchers [9]. Based on the good agreement between the baseline panel analytic and FE/BE approaches [3], the optimized panel was modeled using only analytic techniques.

Modeling

The baseline panel FE model was constructed entirely with solid brick elements. The face sheets were simulated with quasi-isotropic properties computed by integrating through the individual composite layers. The honeycomb core material properties are anisotropic, reflecting the stiffer shear modulus in the ribbon direction. The beams are fastened to the panel model using point spring connections tuned to provide good agreement with measured vibration behavior. The edges of the FE model were grounded to represent a stiff bolted connection to the window frame in the NASA SALT facility. The acoustic BE model was generated using a lumped parameter approach [10], and connected to the FE model so that the radiation damping induced by the surrounding air was properly captured (for stiff lightweight panels with low coincidence frequencies, radiation damping can be substantial). The BE model assumed infinite flat baffles extended from the panel edges.

A Virtual Transmission Loss (VTL) was computed using ARL/Penn State's CHAMP procedure (Combined HydroAcoustic Modeling Programs [11, 12]),

along with structure-borne sound transmission for a transverse point drive at one of the corners of the rib interfaces. To simulate a transmission loss measurement, the panel was excited with a virtual diffuse field pressure. An acoustic diffuse field was applied to both the center panel, and the edge paneling. The center and edge panel regions were loaded separately, so there is no coherence between center and edge regions. Also, although the ribs are fairly large, they were not driven with acoustic loading. Since the spatial correlation of a perfectly diffuse field is a sinc function, the pressure cross-spectral density matrix of the forcing function can be written as

$$G_{FF} = G_{pp} \frac{\boldsymbol{sin}\left(k_0 \Delta_{ij}\right)}{k_0 \Delta_{ij}}, \tag{2}$$

where Δ_{ij} is the separation distance between points i and j, k_o is the acoustic wavenumber and G_{pp} is the power spectral density (PSD) of surface pressure at point i. Assuming unit pressure PSDs at all points, the sound radiation due to the diffuse field was calculated.

To compute a transmission coefficient (radiated power divided by input power), the power incident on the panel was estimated. For a perfectly diffuse field in a room, the power incident on an area S is defined as

$$P_{inc} = \frac{c w_{in}}{4} S, \tag{3}$$

where w_{in} is the reverberant energy density and c is the sound speed. Using the blocked pressure assumption we can approximate w_{in} as

$$w_{in} \cong \frac{|p|^2}{\rho_0 c^2}, \tag{4}$$

where p is the acoustic pressure at the boundary and ρ_o is the fluid density. Since we apply a unit pressure loading to the panel, the squared pressure in Eq. 4 must be

unity. The transmission coefficient then becomes

$$\tau = \frac{P_{rad}}{S / 4\rho_0 c}, \tag{5}$$

where *Prad* is estimated with the BE model. The virtual transmission loss (*VTL*) becomes

$$VTL = 10\,\boldsymbol{log}\left(\frac{S / 4\rho_0 c}{P_{rad}}\right). \tag{6}$$

We also computed the oblique angle of incidence transmission coefficient for an infinite panel, defined as

$$\tau(\phi,\omega) = \frac{\left[2\rho_0 c/\sin\phi\right]^2}{\left[2\rho_0 c/\sin\phi + (D/\omega)\eta\left(k_0\sin\phi\right)^4\right]^2 + \left[\omega\rho h - (D/\omega)\left(k_0\sin\phi\right)^4\right]^2}, \tag{7}$$

where ω is the angular frequency, ϕ is the angle of incidence, *D* is the structural rigidity, η is the structural loss factor and ρh is the plate surface density [13]. For honeycomb sandwich panels, the flexural rigidity is computed as:

$$D = \frac{Et(h+t)^2}{2\left(1-\upsilon^2\right)}, \tag{8}$$

where *E* is the face sheet Young's Modulus, *t* is the face sheet thickness, and *h* is the honeycomb core thickness. Note that *D* increases significantly with core thickness. For the analytic TL calculations, the effects of core shear, which limit the effective panel stiffness, are ignored. Also, we assume the panels are quasi-isotropic for the analytic estimates, and do not consider variable rigidity with orientation. This is consistent with the baseline panel, but the optimized panel does not include layers with 45 degree orientation, so that bending waves not in the 1 or 2 directions will be slower. These effects should be small for the frequencies of interest in this study. For the edge material, *D* is the usual:

$$D = \frac{Et^3}{12\left(1-\upsilon^2\right)}. \tag{9}$$

The diffuse field transmission coefficient over all angles of incidence is then found using:

$$\tau_d(\omega) = \frac{\int_0^{\pi/2} \tau(\phi,\omega)\sin\phi\cos\phi\, d\phi}{\int_0^{\pi/2} \sin\phi\cos\phi\, d\phi} = \int_0^{\pi/2} \tau(\phi,\omega)\sin 2\phi\, d\phi. \tag{10}$$

Note we assume that incident acoustic intensity on the infinite panel is identical over all angles of incidence. This may not be appropriate based on observations in [14, 15], and should be investigated further.

Since there are two panel regions, sound transmission is computed through both. Incident power is computed simply as the product of the surface incident intensity and the panel region areas (30 in x 36 in = 1080 in^2 for the center panel, and 2 x 5 in x 46 in + 2 x 3 in x 36 in = 676 in^2 for the edge regions; see Figure 4 for panel dimensions and subtract a one inch wide frame around the panel when clamped in the NASA SALT facility).

Baseline Panel

Based on vibration measurements, the panel structural loss factors were set to 0.01 (a typical value for sandwich structures). The damping increases at and around panel coincidence, due to the radiation damping simulated in the acoustic BE model. FE/BE and measured surface averaged drive point transverse mobilities (velocity/force) over three locations on the center panel are compared in Figure 15. The resonance frequencies are well captured by the FE/BE model (within 10%), as are the mobilities. The FE/BE mobilities are too low at resonance frequencies below 1 kHz, since the actual measured damping is less than

the assumed 0.01 loss factor. Since this project focuses on frequencies above 1 kHz, this discrepancy was not pursued further. The mobilities also compare well with infinite panel theory estimates, made for both the ribbon (lower bound) and warp (upper bound) directions in the honeycomb core. Figure 16 shows the incident and transmitted power for the baseline panel computed using the FE/BE model (up to 3.2 kHz), and using infinite panel theory. The FE/BE and analytic estimates agree well.

The sound power transmitted through the center panel is highest for frequencies up to 5 kHz, with sound radiated by the edging dominating above 5 kHz. Coincidence peaks in radiated power are evident for the center panel near 600 Hz, and for the edge paneling near 5.5 kHz. FE/BE and analytic TL calculations are compared to measurements made in the NASA SALT facility in Figure 17, which also highlight the important 1 and 3 kHz frequency regions where transmission GMF tones are highest. The measurements and simulations agree well, with the coincidence dip in the analytic model overestimating TL degradation near 5.5 kHz. This is likely because the edging is not really an infinite panel, and analytic theory is only approximate. The similarity between the FE/BE and analytic approach supports the use of analytic theory for assessing optimized panel design concepts (a significant savings in modeling and analysis costs).

Optimized panel

The TL benefits of the split center panel damped design are shown with measured and analytic data in Figure 18. Based on modal analysis measurements, the analytic model assumed structural damping of 0.04 for the center panel and 0.30 for the edge paneling. The optimized panel coincidence dip is higher in frequency, since the split panel cores are half the thickness of that of the baseline

panel (reducing stiffness). As intended, the coincidence dip lies between the two transmission GMF tones at 1 and 3 kHz. The double panel concept nearly doubles TL at 1 kHz, and increases TL by 5 dB at 3 kHz. Note that the mass-spring-mass resonance in the optimized panel, clearly visible in the measured data near 400 Hz, is not modeled in the infinite panel analytic estimate. Figure 19 compares the power radiated by the center and edge panel regions of the optimized panel, and may be used to assess the relative importance of the noise control approaches. The center panel sound radiation is reduced significantly, to the point where it is well below the sound radiated by the edge material at all frequencies except for coincidence near 2 kHz. Also, the impact of the MicroLite blanket is minimal, due to the flanking noise transmission through the edge material. In an actual fuselage, the flanking paths through thin paneling around the sandwich panel roof will also likely dominate sound transmission, so that blankets are not necessary in the split panel design (at least, not for sound insulation purposes).

Along with sound power TL, structure-borne sound transmission was also measured and simulated for a transverse drive applied to one of the corners of the frame. The drive simulates structural forces emanating from the transmission. Figure 20 compares measured sound power for the baseline and optimized panels, and sound power simulated using the FE/BE baseline model. The FE/BE and measured data agree well for the baseline panel. Also, the measured optimized panel sound power transmission is reduced by 6 dB near 1 kHz, and by about 15 dB near 3 kHz.

Summary and Conclusions

An optimized rotorcraft framed roof sandwich panel has been designed to improve sound power TL and structure-borne sound transmission between 1 and 4

kHz, and for two transmission GMF tones at 1 and 3 kHz in particular. The final optimized panel balances acoustic performance with structural integrity constraints, as well as meeting weight and space goals. The optimized split panel concept is augmented with damped face sheets which include embedded VHB viscoelastic material, and is filled with a MicroLite blanket. The air gap is sufficiently thick so that the mass-spring-mass panel resonance is well below the lowest frequency range of interest. Although the optimized panel is thicker than the baseline panel, the excess thickness is shifted to outside the fuselage, and will not affect the transmission or other electrical, mechanical, or hydraulic elements in the roof cavity region.

The optimized panel was constructed, and then tested in NASA's SALT facility to confirm the simulated TL improvements. The optimized panel reduces acoustically transmitted sound by 6-11 dB, and also reduces structurally-transmitted sound by 6-15 dB. However, the sound transmitted through the center sandwich panel region was reduced so much that the edge panel radiation became dominant. The edge radiation masks most additional noise reduction from the Microlite fill material, which may not be necessary in future designs for actual rotorcraft.

FE/BE modeling of the TL and structure-borne radiated sound of the baseline panel matches measurements within 3 dB. However, simple analytic TL modeling also matches measured data within 3 dB over most frequencies. The analytic theory may therefore be used for future TL design studies at significant time and cost savings.

Acknowledgements

The authors thank NASA for their support under NASA Contract

#NNL11AA02C, under NRA NNH09ZEA001N, Subtopic A.3.3.1: Fundamental Vibro-Acoustic Modeling and Validation. We also thank David Gries of the 3M corporation for suggesting the use of VHB 9469 viscoelastic material.

References

1. Hambric, S.A., Shepherd, M.R., Campbell, R.L., and Hanford, A.D., Simulations and measurements of the vibroacoustic effects of replacing rolling element bearings with journal bearings in a simple gearbox," *ASME J. Vib. Ac.*, 135, June 2013.
2. Hambric, S.A., Smith, E.C., Szefi, J.T., and Campbell, R.L., Helicopter transmission noise mechanisms, analysis methods, and noise reduction techniques, *Proceedings of NoiseCon 2004*, Baltimore, Maryland, July 2004.
3. Hambric, S.A., Shepherd, M.R., May, C., and Snider, R., Acoustically Tailored Composite Rotorcraft Fuselage Panels, *NASA/CR-2015-218769*, July 2015.
4. Grosveld, F.W.. Calibration of the structural acoustics loads and transmission facility at NASA Langley Research Center. Proc. INTER-NOISE 99; 6-8 December 1999; Fort Lauderdale, Florida, 1999.
5. Davis, E.B., "Designing Honeycomb Panels for Noise Control," AIAA/CEAS Aeroacoustics Conference, A99-27801, 792-800, 1999.
6. Peters, P.R., Rajaram, S., and Nutt, S., "Sound transmission loss of damped honeycomb sandwich panels," Proceedings of Internoise 2006, Honolulu, HI, 3-6 December 2006.
7. J. Loughlin, "Honeycomb plate properties," *Finite element modeling continuous improvement: the book*, NASA Goddard Space Flight Center, code 542 e-book, http://femci.gsfc.nasa.gov/hcplate/index.html .
8. Hambric, S.A., Fahnline, J.B., Campbell, R.L., Shepherd, M.R., and Conlon, S.C., "Modal based experimental vibro-acoustic analysis of sandwich panels," *Proceedings of NOVEM 2015*, Dubrovnik, Croatia, 13-15 April 2015 (available

online at INCE-USA digital publications site).

9. Zhou R. and Crocker, M.J. “Boundary element analyses for sound transmission loss of panels,” *J. Acoust. Soc. Am.* **127 (2)**, 829-840, 2010.
10. Koopmann, G.H., and Fahnline, J.B., *Designing Quiet Structures*, Academic Press, 1997.
11. Hambric, S.A., Jonson, M.L., Fahnline, J.B. and Campbell R.L., "Simulating the vibro-acoustic power of fluid-loaded structures excited by randomly distributed fluctuating forces," *Proceedings of NOVEM 2005*, St. Raphael, France, 18-21 April 2005.
12. Hambric, S.A., Boger, D.A., Fahnline, J.B., and Campbell, R.L., "Structure- and fluid-borne acoustic power sources induced by turbulent flow in 90 degree piping elbows," *Journal of Fluids and Structures*, 26, 121-147, 2010.
13. Fahy, F., and Gardonio, P., *Sound and Structural Vibration, second edition*, Academic Press, 2007.
14. Lynch, K., Bauch, P., Hambric, S., and Barnard, A., “A proposed correction for incident sound intensity distribution for diffuse field panel excitation and transmission loss simulations,” *Proceedings of NoiseCon 2014*, Fort Lauderdale, Florida, 8-10 September 2014.
15. Kang, H.J., Ih, J.G., Kim, H.S., and Kim, J.S., “An experimental investigation on the directional distribution of incident energy for the prediction of sound transmission loss,” *Applied Acoustics*, 63, 283-294, 2002.

List of Figures

List of Tables

Figure 1 – View of the inside of the transmission region in a commercial rotorcraft.

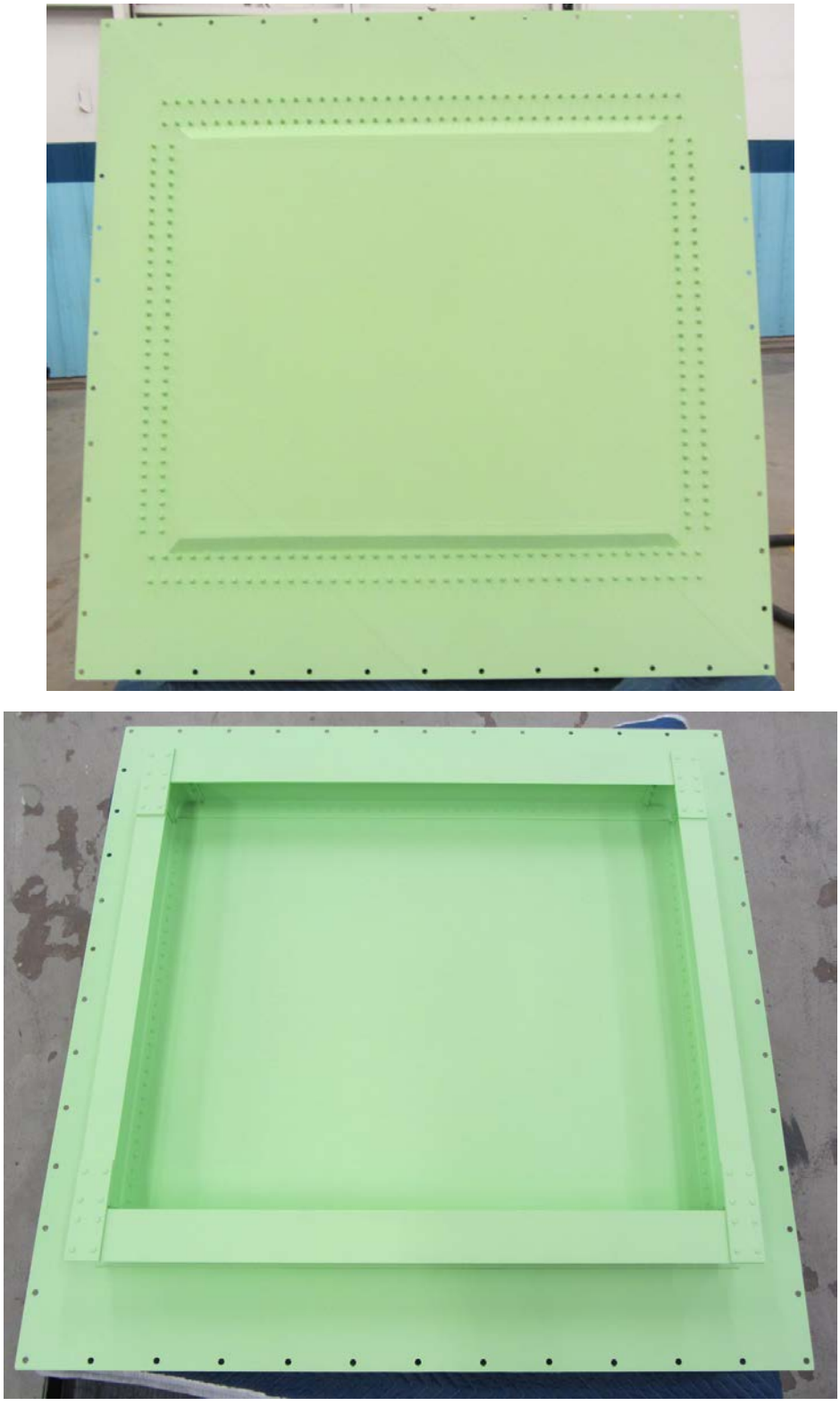

Figure 2 – Interior (top) and exterior (bottom, with frame) views of the notional baseline roof panel.

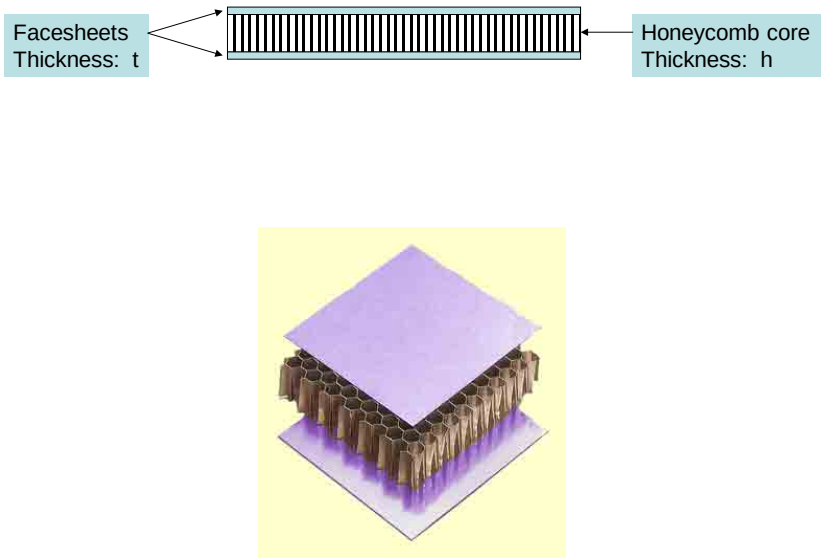

Figure 3 – Schematic of typical honeycomb core/composite facesheet panel.

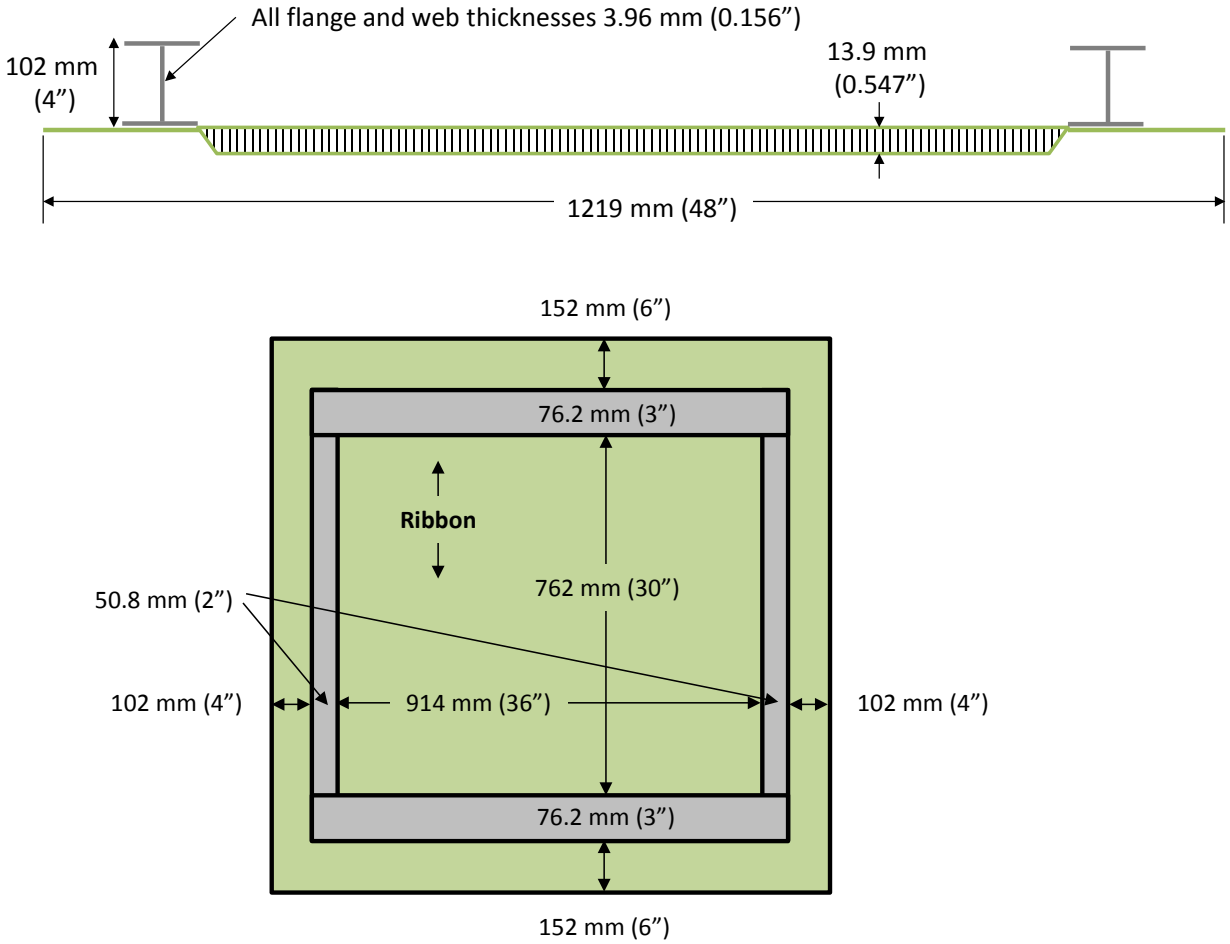

Figure 4 – Baseline panel dimensions (not to scale). Optimized panel has same in-plane dimensions and beams but different cross section.

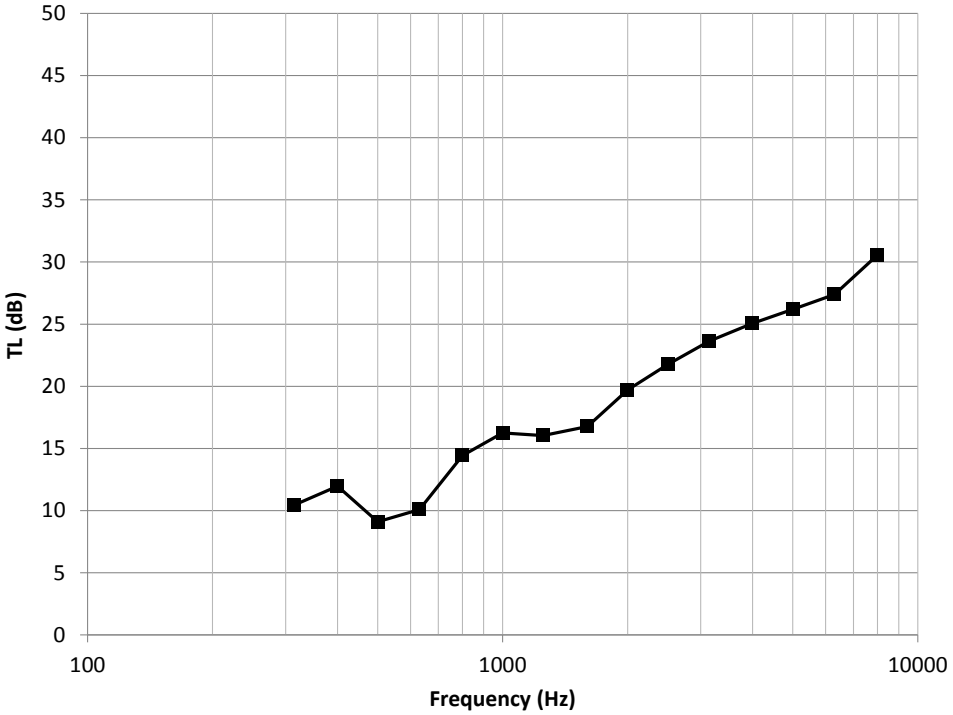

Figure 5 – Measured TL (at NASA's SALT facility [4]) for diffuse acoustic drive.

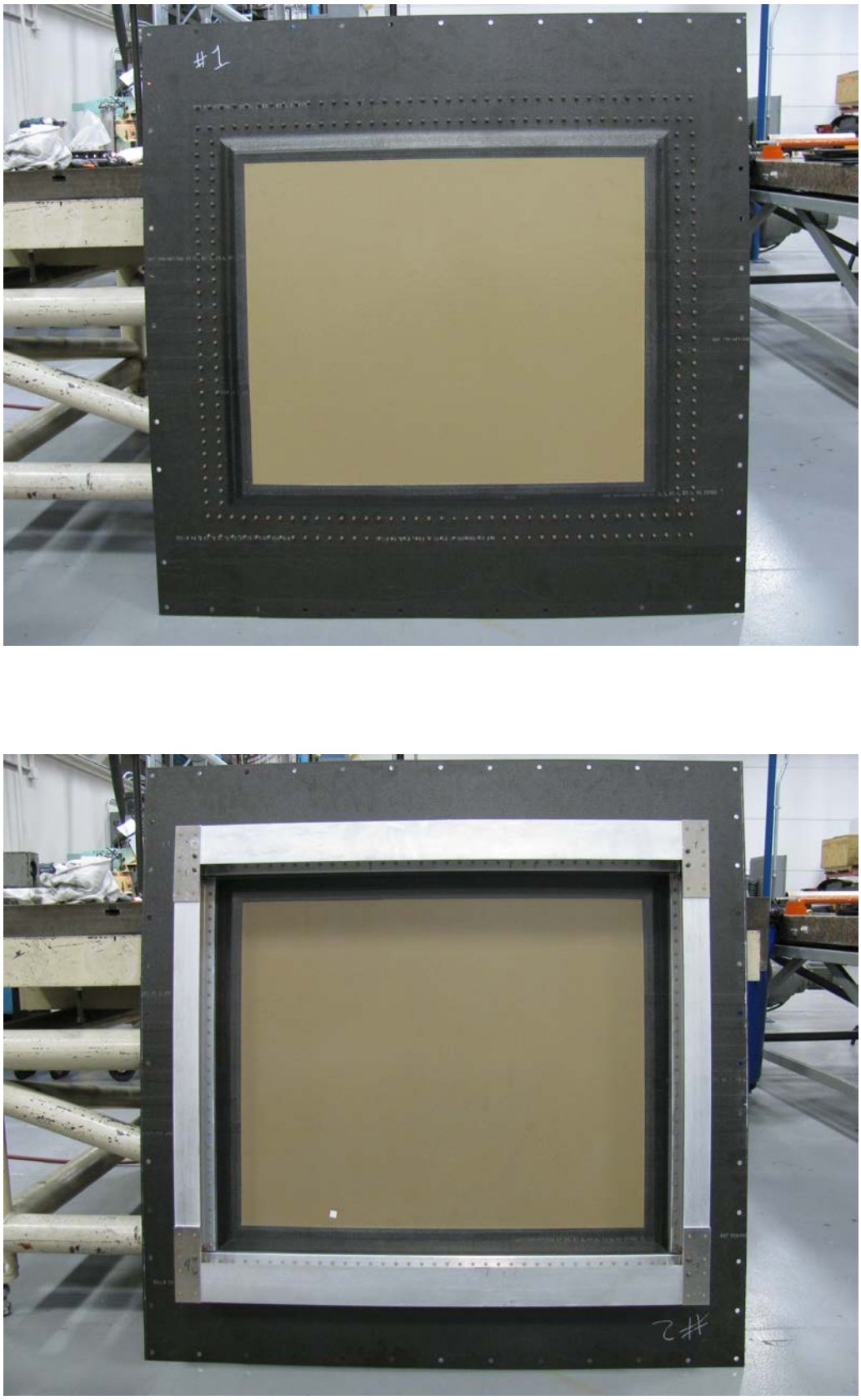

Figure 6 – Interior (top) and exterior (bottom, with frame) views of the optimized roof panel.

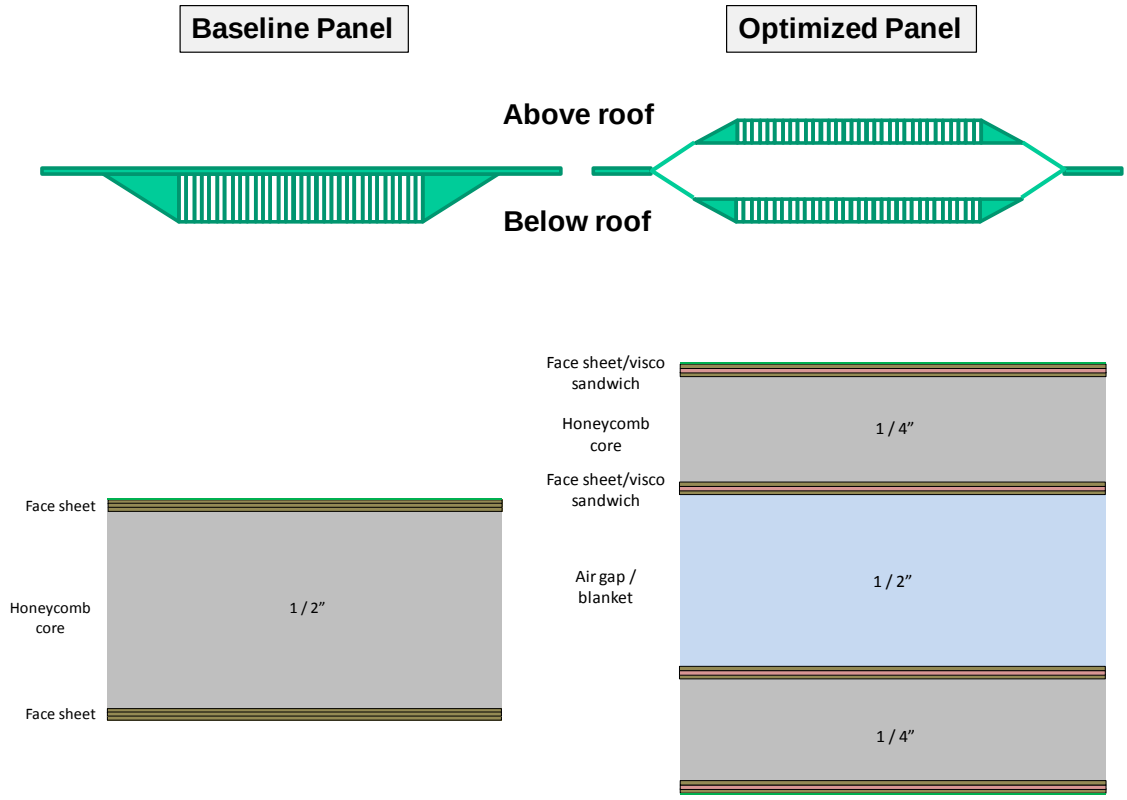

Figure 7 – Schematics and cross sections of baseline (left) and optimized (right) panels (not to scale).

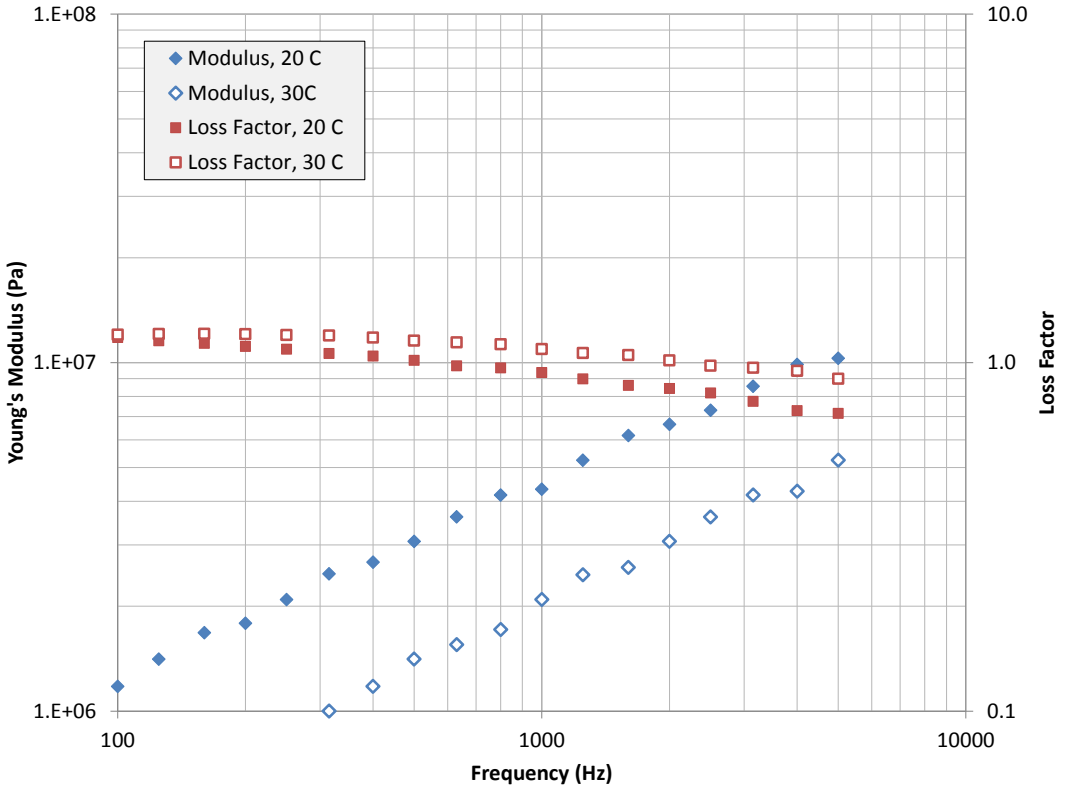

Figure 8 – Young's modulus and loss factor for 3M VHB 9469 at 20 C and 30 C.

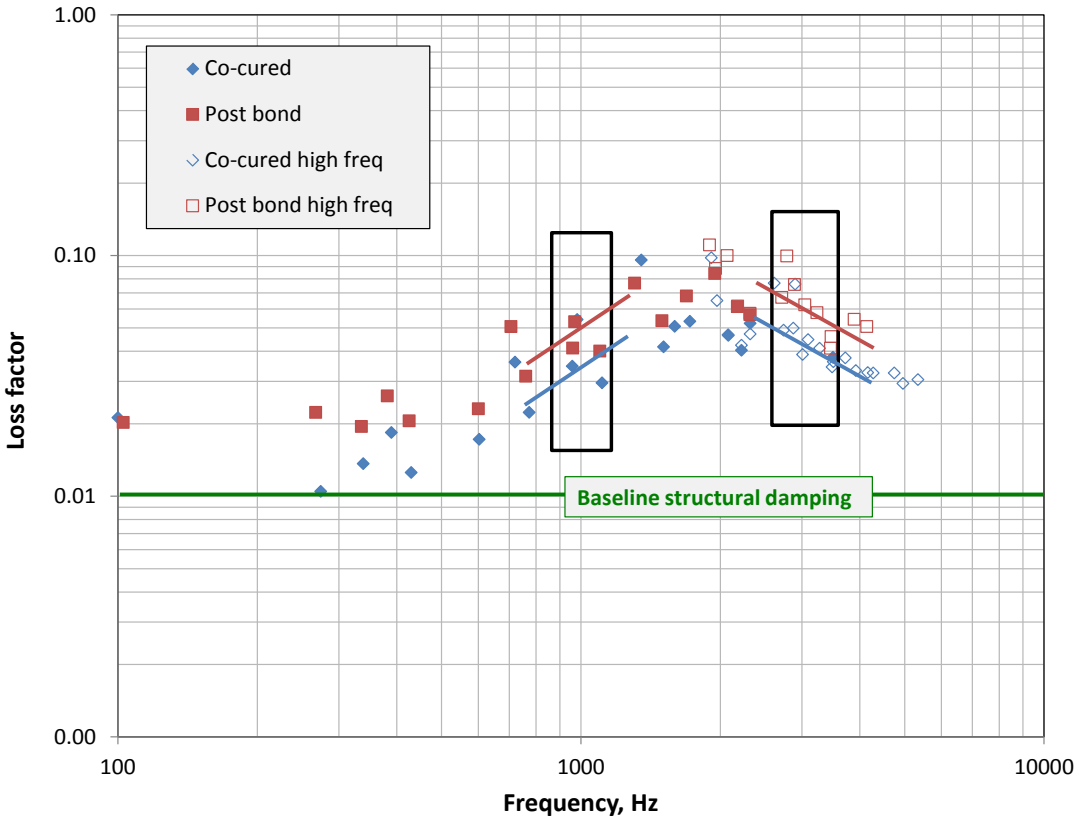

Figure 9 – Measured structural loss factors for two test coupons with embedded VHB 9469.

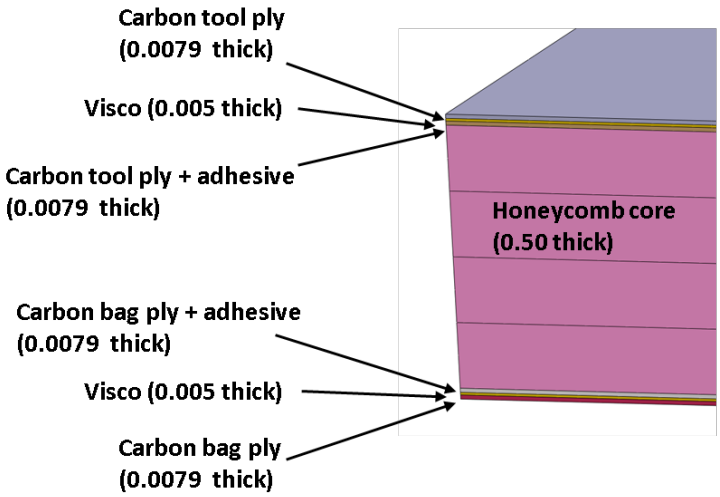

Figure 10 – Cross-sectional detail of the FEM model for test coupons with embedded VHB material.

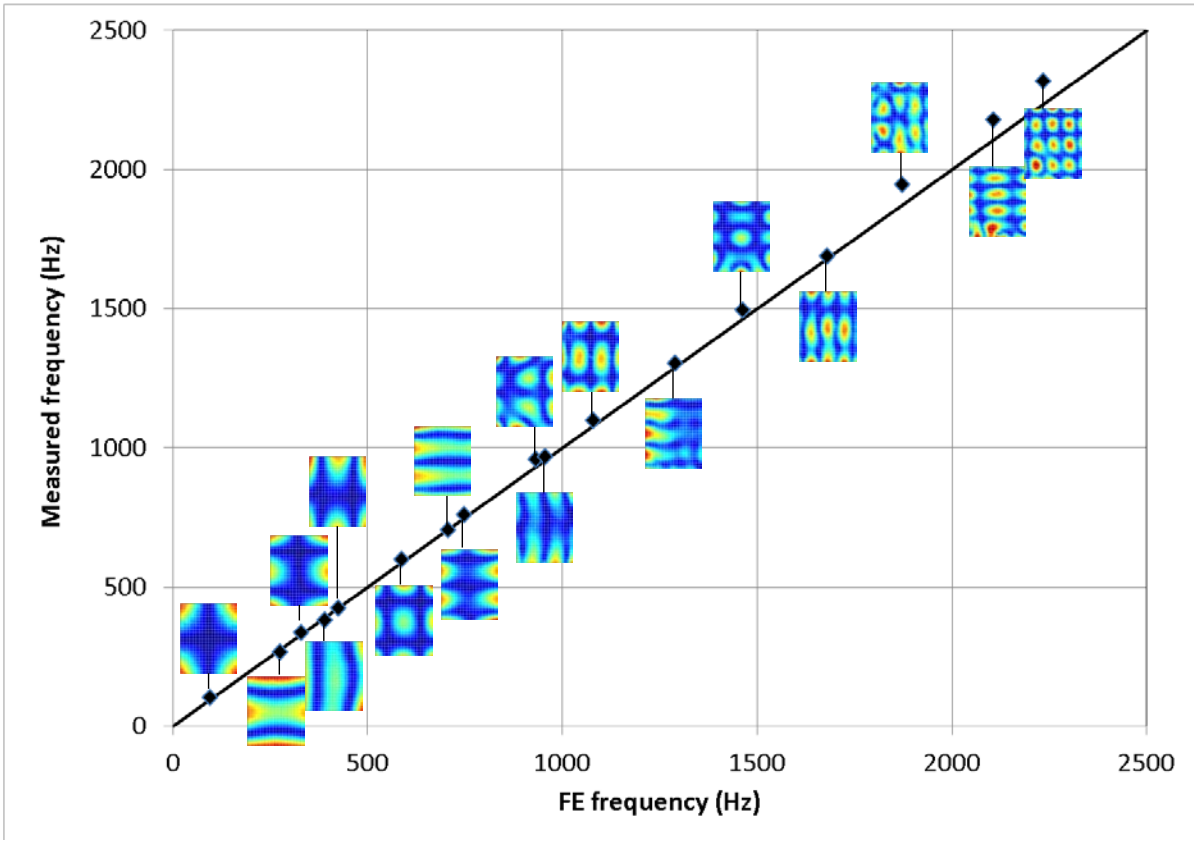

Figure 11 – FE vs. measured resonance frequencies for several mode shapes for test coupon with embedded VHB 9469.

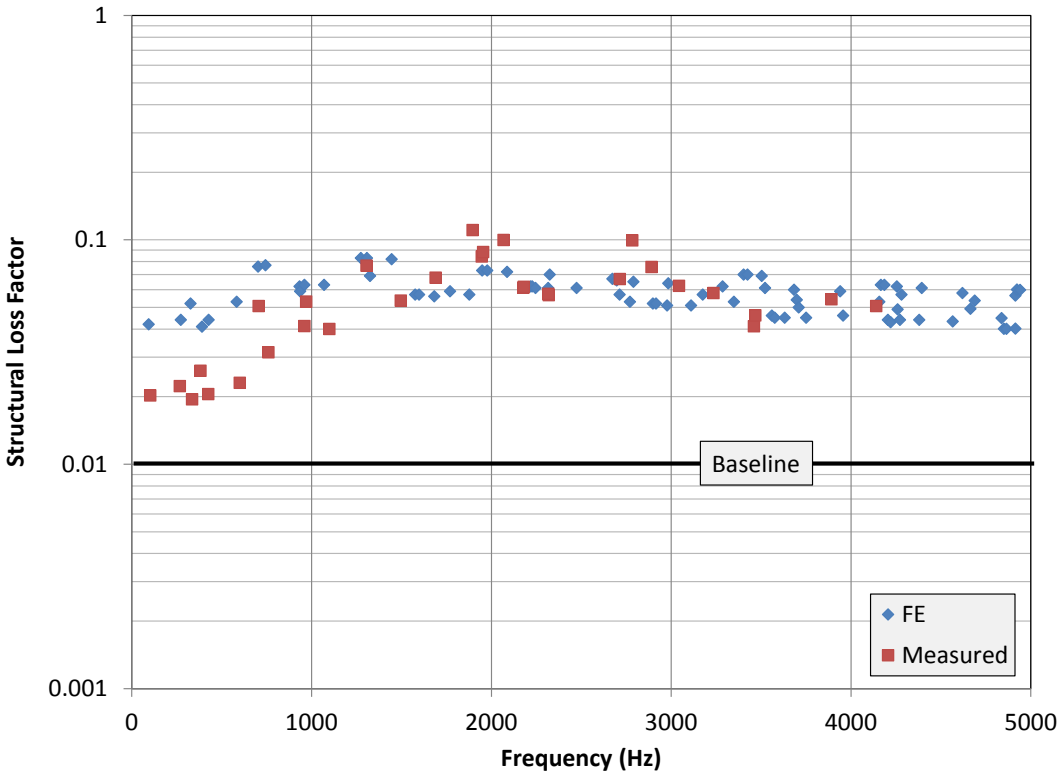

Figure 12 – FE vs. measured damping loss factors for test coupon with embedded VHB 9469.

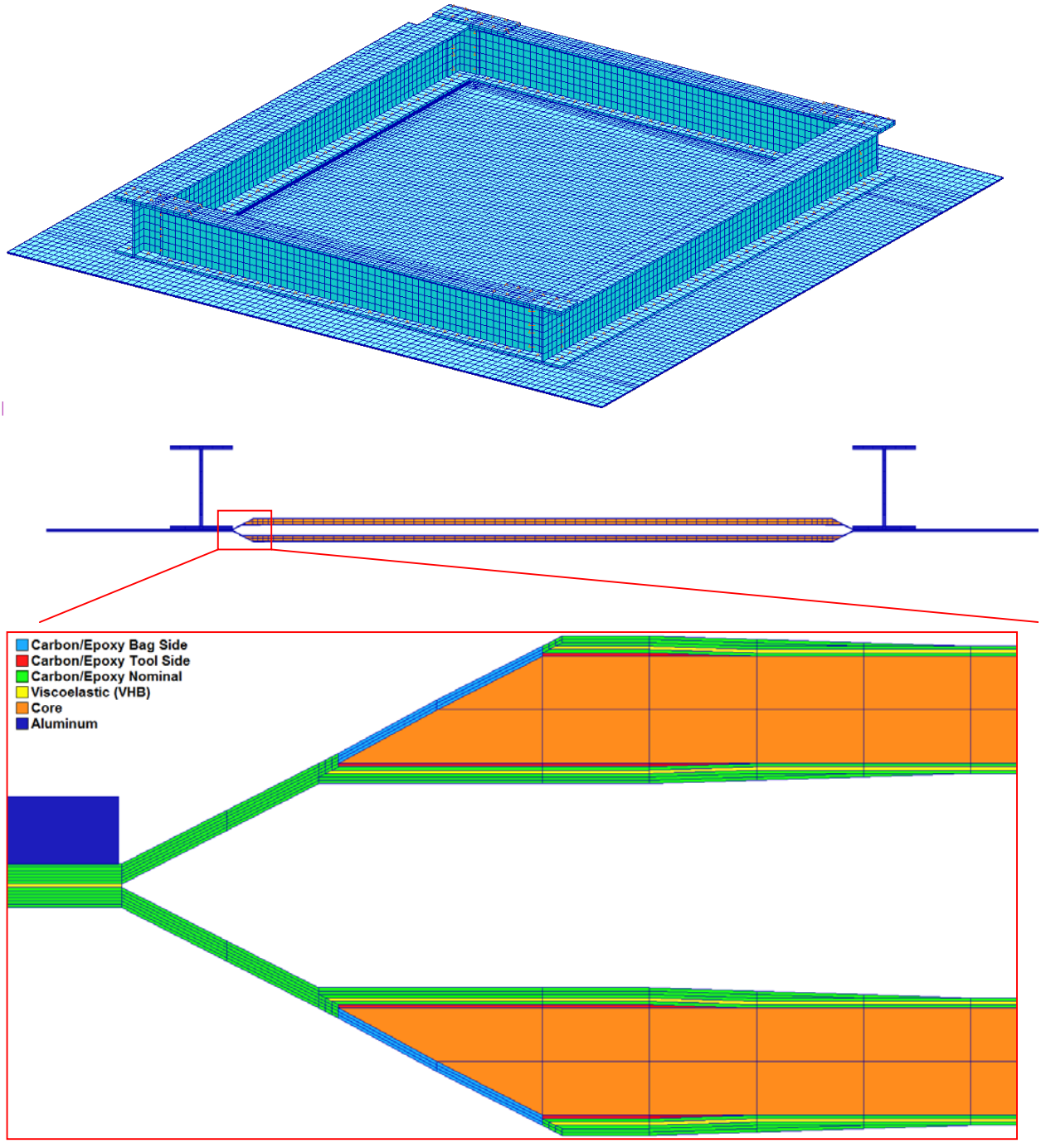

Figure 13 – FE model of optimized panel.

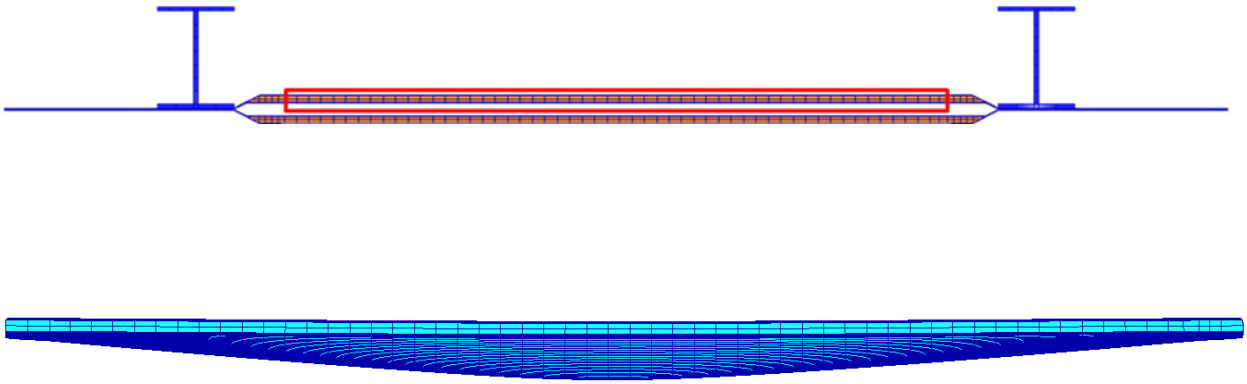

Figure 14 – Top: Panel section for step load analysis highlighted in red box;

Bottom: Non-linear analysis deflection results.

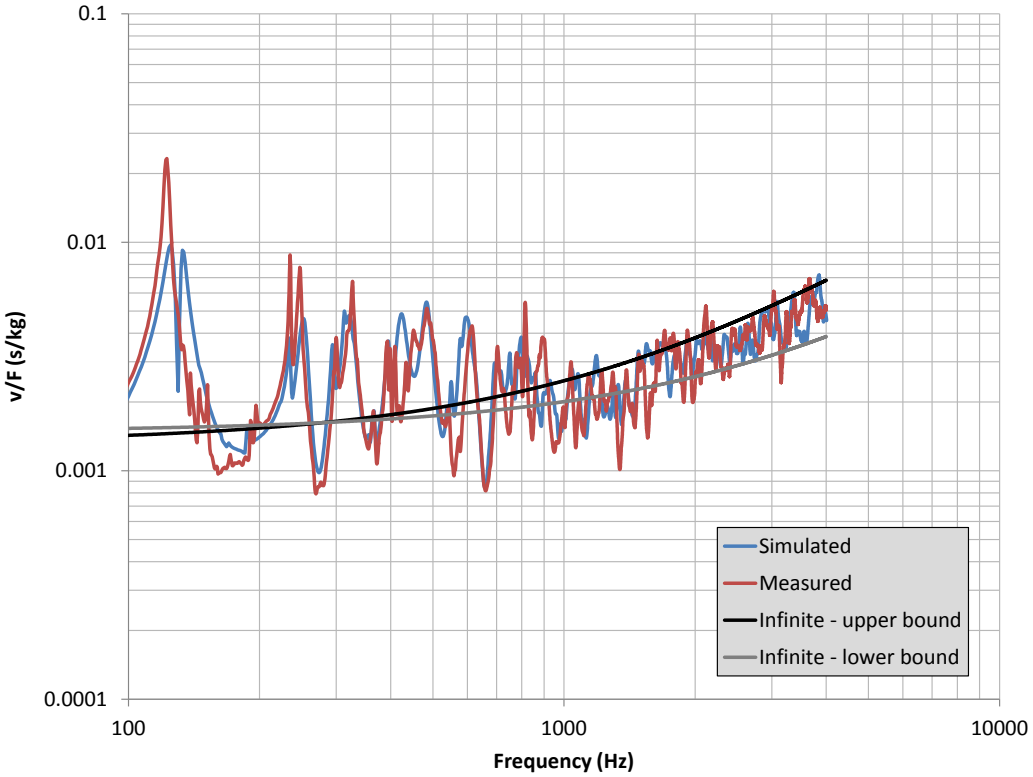

Figure 15 – Measured and simulated surface-averaged drive point mobility over center panel.

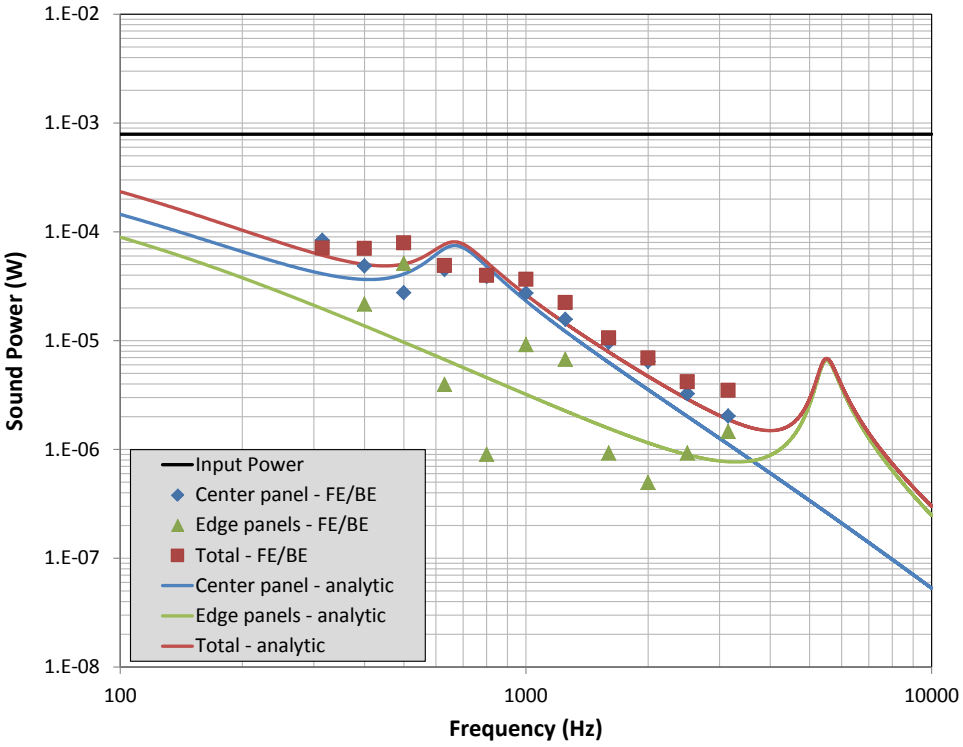

Figure 16 – Simulated input and radiated sound power for baseline panel.

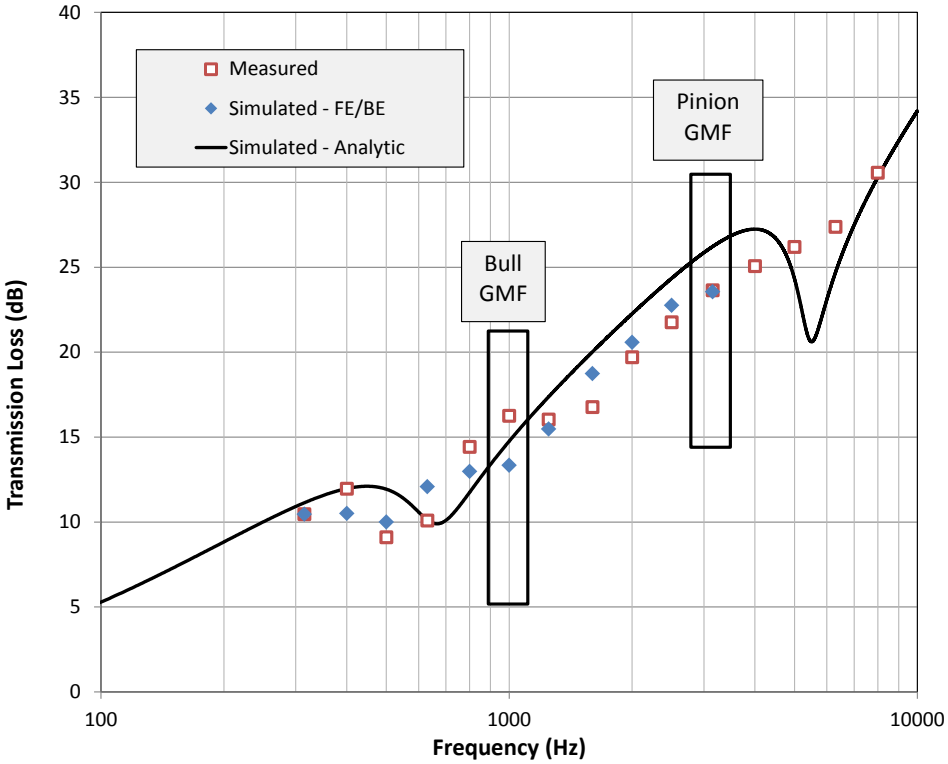

Figure 17 – Measured and simulated TL for baseline panel.

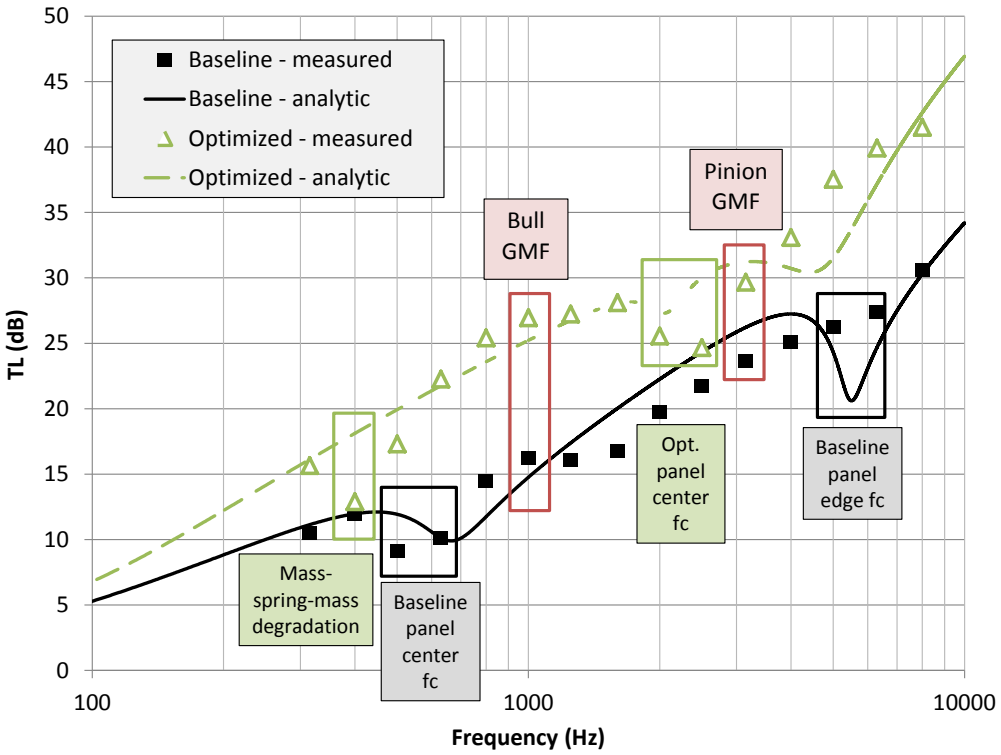

Figure 18 – TL of baseline and optimized panels, simulations and measurements.

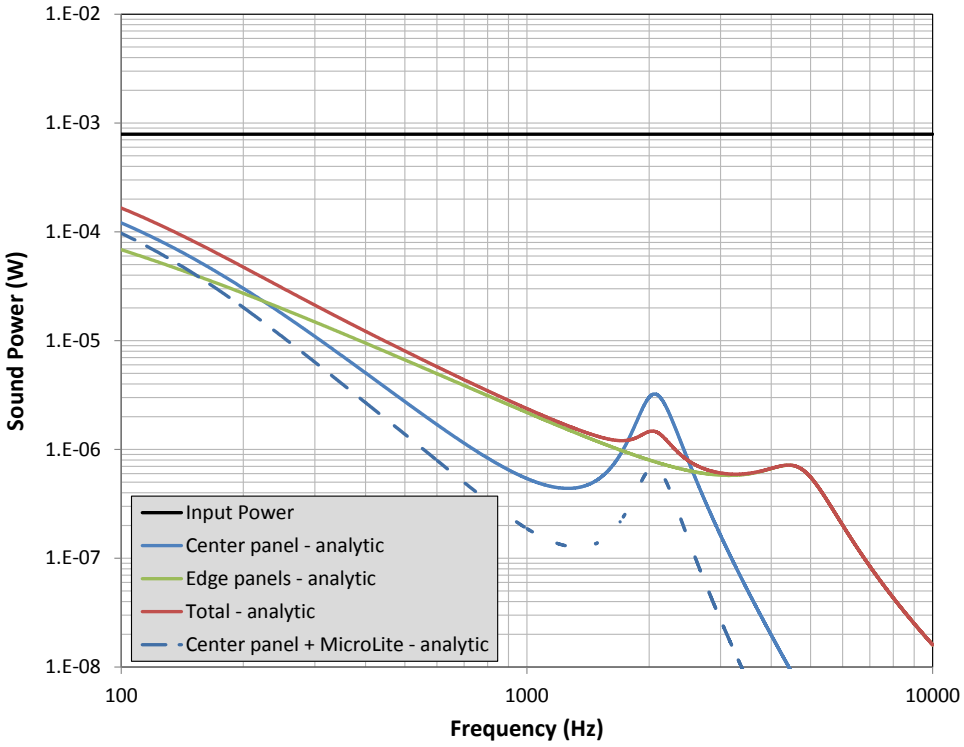

Figure 19 – Incident and transmitted powers for optimized panel.

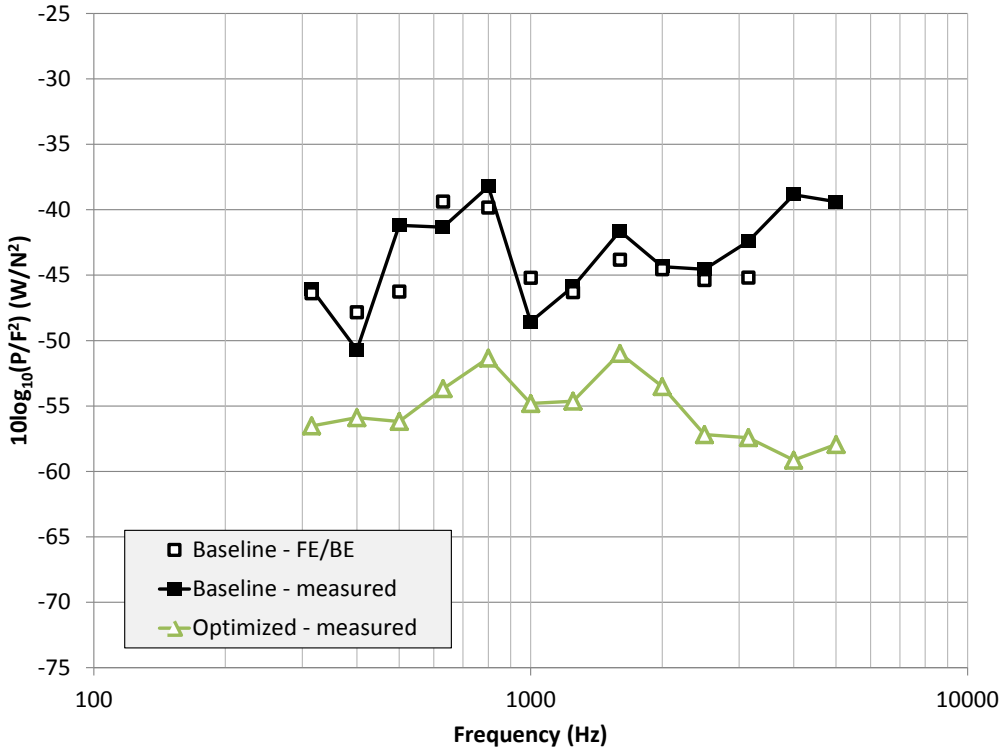

Figure 20 – Measured structure-borne radiated sound power for joint transverse drive on baseline (including FE/BE) and split center panel designs.

Tables

Table 1a – Selected center sandwich panel material properties. The 1 and 2 directions are in-plane.

Property	Face Sheets	Kevlar Core
E_{11}, E_{22} (GPa/Msi)	57 / 8.3	-
ν_{12}	0.21	-
G_{13} (MPa/ksi)	-	139 / 20.1 (ribbon)
G_{23} (MPa/ksi)	-	68 / 9.8 (warp)
ρ (kg/m^3 / lb/in^3)	1550 / 0.0560	47 / 0.0017

Table 1b – Edge panel properties. The 1 and 2 directions are in-plane.

Property	Value
E_{11}, E_{22} (GPa/Msi) - baseline	54 / 7.8
E_{11}, E_{22} (GPa/Msi) - optimized	43 / 6.2
ν_{12}	0.21
ρ (kg/m^3 / lb/in^3)	1550 / 0.0560
t (mm / in) - baseline	2.0 / .079
t (mm / in) - optimized	2.5 / .098

Table 2 – Effects of air gap thickness on mass-spring resonance frequency and overall panel thickness.

Air gap thickness (mm/in)	Resonance Frequency (Hz)	Overall panel thickness (mm/in)
3.18 / 0.125	911	18.0 / 0.709
6.35 / 0.25	644	21.2 / 0.835
12.7 / 0.5	456	27.5 / 1.083

Table 3 – Measured and mass-law based sound transmission loss improvements due to use of Microlite.

Frequency (Hz)	dB, Measured by Vendor	dB, Mass Law
500	2.4	2.4
1000	4.6	4.7
2000	6.6	6.8
4000	8.8	10.5